INFECTION AND IMMUNITY, Oct. 2011, p. 3978–3992 Vol. 79, No. 10
0019-9567/11/$12.00 doi:10.1128/IAI.00192-11

Targeted Disruption of Nonribosomal Peptide Synthetase *pes3* Augments the Virulence of *Aspergillus fumigatus*▽†

Karen A. O'Hanlon,[1] Timothy Cairns,[2] Deirdre Stack,[1] Markus Schrettl,[1,3] Elaine M. Bignell,[2] Kevin Kavanagh,[1] Sinéad M. Miggin,[1,4] Grainne O'Keeffe,[1] Thomas O. Larsen,[5] and Sean Doyle[1]*

Department of Biology and National Institute for Cellular Biotechnology, National University of Ireland Maynooth, Co. Kildare, Ireland[1]; Department of Microbiology, Imperial College London, London SW7 2AZ, United Kingdom[2]; Division of Molecular Biology/Biocenter, Innsbruck Medical University, Innsbruck, Austria[3]; Institute of Immunology and Department of Biology, National University of Ireland Maynooth, Co. Kildare, Ireland[4]; and Center for Microbial Biotechnology, DTU Systems Biology, Technical University of Denmark, DK-2800, Kgs, Lyngby, Denmark[5]

Received 24 February 2011/Returned for modification 15 March 2011/Accepted 28 June 2011

Nonribosomal peptide synthesis (NRPS) is a documented virulence factor for the opportunistic pathogen *Aspergillus fumigatus* and other fungi. Secreted or intracellularly located NRP products include the toxic molecule gliotoxin and the iron-chelating siderophores triacetylfusarinine C and ferricrocin. No structural or immunologically relevant NRP products have been identified in the organism. We investigated the function of the largest gene in *A. fumigatus*, which encodes the NRP synthetase Pes3 (AFUA_5G12730), by targeted gene deletion and extensive phenotypic analysis. It was observed that in contrast to other NRP synthetases, deletion of *pes3* significantly increases the virulence of *A. fumigatus*, whereby the *pes3* deletion strain (*A. fumigatus* Δ*pes3*) exhibited heightened virulence (increased killing) in invertebrate ($P < 0.001$) and increased fungal burden ($P = 0.008$) in a corticosteroid model of murine pulmonary aspergillosis. Complementation restored the wild-type phenotype in the invertebrate model. Deletion of *pes3* also resulted in increased susceptibility to the antifungal, voriconazole ($P < 0.01$), shorter germlings, and significantly reduced surface β-glucan ($P = 0.0325$). Extensive metabolite profiling revealed that Pes3 does not produce a secreted or intracellularly stored NRP in *A. fumigatus*. Macrophage infections and histological analysis of infected murine tissue indicate that Δ*pes3* heightened virulence appears to be mediated by aberrant innate immune recognition of the fungus. Proteome alterations in *A. fumigatus* Δ*pes3* strongly suggest impaired germination capacity. Uniquely, our data strongly indicate a structural role for the Pes3-encoded NRP, a finding that appears to be novel for an NRP synthetase.

Aspergillus fumigatus is an opportunistic pathogen of immunocompromised individuals, exhibiting a 50 to 95% mortality rate, with the severity of disease depending on the immune status of the host (1, 17, 35). Nonribosomal peptide synthesis (NRPS) is a key mechanism for the biosynthesis of bioactive metabolites in bacteria and fungi (45, 50) and has been found to contribute to *A. fumigatus* virulence (1). Sequencing of the *A. fumigatus* genome has revealed the presence of at least 14 genes encoding putative nonribosomal peptide (NRP) synthetases (16, 50). NRP synthetases are modular or multimodular enzymes that direct the biosynthesis of NRPs independently of the ribosome (38, 66). Together with polyketides and terpenoids, NRPs constitute a class of structurally diverse secondary metabolites, which are generally considered to be components of the chemical arsenal necessary for adaptation to ecological niches (11, 22).

Each module within an NRP synthetase is responsible for the recognition, via an adenylation (A) domain, and incorporation of a single amino acid into the cognate peptide product (66); however, the basis of this recognition system is poorly understood. Furthermore, elucidating the specific NRP synthetase responsible for directing the biosynthesis of an NRP is nontrivial and defining the primary biochemical function of the NRP is challenging. Therefore, because few fungus-specific A domain substrates and NRP roles, particularly in *A. fumigatus*, have been established to date (20), it is imperative to assign functionality to the fungal NRP products. A few *A. fumigatus* NRP synthetases encoding secreted or intracellularly located peptides have been elucidated to date, mainly facilitated through targeted gene deletion and comparative metabolomic studies. Two NRP synthetases, SidC and SidD, were found to be essential for siderophore biosynthesis in *A. fumigatus* (58, 60). GliP, a bimodular NRP synthetase, was shown to be responsible for gliotoxin biosynthesis (5, 15); however, the contribution to organismal virulence remains to be definitely established. FtmA (brevianamide F synthetase) makes the diketopiperazine scaffold, brevianamide F, which is the precursor of the fumitremorgin family of tremorgenic secondary metabolites (39). A multimodular NRP synthetase *pes1* was identified to be important for virulence and protection against oxidative stress (57). Importantly, where virulence studies have been undertaken, the disruption of a particular NRP synthetase has generally led to virulence attenuation, highlighting the

* Corresponding author. Mailing address: Department of Biology and National Institute for Cellular Biotechnology, National University of Ireland Maynooth, Co. Kildare, Ireland. Phone: 353-1-7083858. Fax: 353-1-7083845. E-mail: sean.doyle@nuim.ie.

† Supplemental material for this article may be found at http://iai.asm.org/.

▽ Published ahead of print on 11 July 2011.

importance of NRPS in the pathogenicity of *A. fumigatus* and other fungi (51, 57, 60, 68). To our knowledge, no structural role for an *A. fumigatus* NRP has been identified or proposed to date.

pes3 (CADRE locus identifier, AFUA_5G12730 [http://www.cadre-genomes.org.uk/index.html]; NRPS8 [16]), encoding a multimodular NRP synthetase (8,515 amino acids), is the largest gene (25 kb) in *A. fumigatus*, representing 0.01% of the genome (16, 65, 66). In addition, a recombinant Pes3 module was a target for posttranslational modification via solid-phase 4′-phosphopantetheinylation, thereby confirming the likelihood of *in vivo* functionalization via this process (65). BLAST searching of *pes3* revealed no sequence orthologs in any organism for which the full genome sequence is available, making it difficult to predict the NRP produced by Pes3 by comparison to other organisms (16, 66). Pes3 contains six A domains and is predicted to encode a peptide with 6 amino acids, if each A domain exhibits unique substrate specificity. However, it has been proposed that the nonlinear modular and domain arrangement of Pes3 may suggest repetitive or nonlinear use of modules (16), confounding *in silico* prediction of cognate NRP structure, location, and function (45). Phylogenomic and expression analysis of all *A. fumigatus* NRP synthetase genes revealed that *pes3* exhibited a unique pattern of expression compared to all other *A. fumigatus* NRP synthetase genes, whereby *pes3* transcripts were most abundant in ungerminated spores, in contrast to all other NRP synthetase genes examined (16). This suggested that *pes3* may be involved in germination; however, no further characterization of *pes3* was carried out during that study.

We set out here to identify the role of the NRP synthetase Pes3 in *A. fumigatus* and to assess its contribution to virulence. Disruption of *pes3* (resulting in a Δ*pes3* strain) resulted in an augmented virulence phenotype in invertebrate and hydrocortisone acetate immunosuppressed models for invasive aspergillosis (IA). Unexpectedly, this virulence appears to be mediated by an immunologically silenced phenotype for Δ*pes3*. We propose that Pes3 biosynthesizes an NRP with a structural role within *A. fumigatus* conidia that is essential for effective innate immune recognition.

MATERIALS AND METHODS

Strains, growth conditions, and general DNA manipulation. *A. fumigatus* strains were grown at 37°C in *Aspergillus* minimal medium (AMM), and fungal culturing was carried out as described in Schrettl et al. (61). Fungal strains used in the present study are listed in Table 1.

PCRs for generation of DNA manipulation constructs were performed using the Expand long-range template kit (Roche). For general cloning procedures, the bacterial strain *Escherichia coli* DH5α was used (33); this strain was cultivated in LB (1% Bacto tryptone, 0.5% yeast extract, 1% NaCl [pH 7.5]) medium. *A. fumigatus* genomic DNA was purified using a ZR fungal/bacterial DNA kit (Zymoresearch).

Gene deletion and complementation of *A. fumigatus pes3*. *A. fumigatus* transformation was carried out according to the method of Tilburn et al. (70). For the disruption of *pes3* and generation of the Δ*pes3* mutant strain, a bipartite marker technique was used (49). The strategy designed for *pes3* disruption in the present study led to the deletion of 1.5 kb of *pes3* at the 5′ region of the gene. In *A. fumigatus* Δ*pes3*, the deleted region comprises amino acids 688 to 1163 of *pes3*.

Briefly, *A. fumigatus* ATCC 46645 was transformed with two DNA constructs, each containing an incomplete fragment of a pyrithiamine resistance gene (*ptrA*) (31, 32), fused to 1.2 and 1.3 kb of the *pes3* coding sequences, respectively, which flanked the region to be deleted. The marker fragments shared a 557-bp overlap within *ptrA*, serving as a potential recombination site during transformation. Two rounds of PCR generated each fragment. Table 2 provides a complete list of the primers used in the present study. First, each flanking region was amplified from ATCC 46645 genomic DNA by using the primer pair oAf*pes3*-1 and oAf*pes3*-4 for flanking region A (1.2 kb) and the primer pair oAf*pes3*-2 and oAf*pes3*-3 for flanking region B (1.3 kb). Subsequent to gel purification, the fragments were digested with EcolCRI and HindIII, respectively. The *ptrA* selection marker was released from plasmid pSK275 (kindly provided by Sven Krappmann, Goettingen, Germany) by digestion with EcolCRI and HindIII and ligated with the two flanking regions A and B described above. For transformation, two overlapping fragments were amplified from the ligation products by using the primers oAf*pes3*-5 and o*ptrA*-2 for fragment C (2.6 kb) and the primers oAf*pes3*-6 and o*ptrA*-1 for fragment D (2.3 kb). Subsequently, *A. fumigatus* ATCC 46645 was transformed simultaneously with the overlapping fragments C and D. In order to obtain homokaryotic transformants, colonies from single homokaryotic spores were picked, and single genomic integration was confirmed by PCR (data not shown) and Southern blot analysis.

TABLE 1. Fungal strains and plasmid constructs

Strain or plasmid	Description	Source or reference
Strains		
ATCC 46645	*Aspergillus fumigatus* wild-type strain	24
pes3	Δ*pes3* deletion mutant (*pes3*::*ptrA*)	This study
pes3^{C}	*pes3* complemented strain	This study
Plasmids		
pSK275	Plasmid containing *ptrA* cassette conferring resistance to pyrithiamine	30
pAN 8.1	*Aspergillus* marker cassette conferring resistance to phleomycin (*^{P}gpdA*::*ble*/*tk*::*trpC*)	

For complementation of *A. fumigatus* Δ*pes3*, a bipartite strategy was also used to precisely replace the deleted region in Δ*pes3*, thus leading to *pes3*^{C}. Two overlapping PCR fragments were amplified by using the primer pairs oAf*pes3*-5/*Afpes3*Comp1 (fragment 1) and *Afpes3*Comp2/oAf*pes3*-6 (fragment 2) (Table 2). These fragments overlapped by 405 bp, and recombination of these fragments should restore *pes3*, resulting in the removal of *ptrA* from the genome of *pes3*^{C}. To achieve this, *A. fumigatus* Δ*pes3* was cotransformed with fragments 1 and 2 and a plasmid, Pan8.1, containing a phleomycin resistance gene (*ble*^{r}) for selection. Positive deletion and reconstituted strains were screened by Southern analysis, and digoxigenin-hybridization probes were generated by using the primers oAf*pes3*-5 and oAf*pes3*-4 (Table 2). Complementation of *pes3* was further verified by restriction mapping part of the *pes3* locus. PCR was carried out using the primer pair oAf*pes3*-5 and oAf*pes3*-6, and either wild-type, Δ*pes3* or *pes3*^{C} genomic DNA as a template, leading to PCR products spanning the specific area of *pes3* that was targeted for deletion (3,737 bp in wild-type and *pes3*^{C} strains and 4,285 bp in the Δ*pes3* strain). These PCR products were restricted with AgeI to yield a range of expected fragment sizes as detailed in Table 3.

RNA isolation and real-time PCR. Fungal RNA was isolated and purified from *A. fumigatus* hyphae crushed in liquid nitrogen by using the RNeasy plant minikit (Qiagen). RNA was treated with DNase 1 (Invitrogen), and cDNA synthesis from mRNA (500 ng) was performed using a first-strand transcription cDNA synthesis kit (Roche) with oligo(dT) primers. The gene encoding calmodulin (*calm*) (AFUA_4G10050), which is constitutively expressed in *A. fumigatus*, served as a control in reverse transcription-PCR (RT-PCR) experiments (10).

Real-time PCR was performed using LightCycler 480 Sybr green 1 master mix (Roche) on a LightCycler 480 real-time PCR system. PCRs were carried out in 96-well plates in a reaction volume of 20 μl containing 5 μl of template cDNA. Standard curves were prepared for *calm* and *pes3* by generating 5 orders of 10-fold serial dilutions of cDNA in H_2O and performing five replicate PCRs on these dilutions. The primer pairs *calm F*/*calm R* or *Pes3*RT-F/*Pes3*RT-R were used for real-time PCR experiments (Table 2). Cycling conditions for PCRs were calculated using the recommendations from Roche, and 40 cycles of PCR were performed. Standard curves with a PCR efficiency of ≥1.8 and with an error value of <0.2 were accepted, and the cycling conditions were used for subsequent real-time PCR analysis by relative quantification using LightCycler 480 software. For real-time PCRs, a 1/10 dilution of cDNA from each sample was used as a template, and each reaction was performed in triplicate.

Metabolite extraction and analysis by reversed-phase HPLC. Metabolite extraction was performed according to the micro extraction procedure of Smedsgaard

TABLE 2. Oligonucleotides used in this study

Primer	Orientation[a]	Sequence (5′–3′)	PCR usage
o*Afpes3*-1	F	GAGGCGGAACGTTGGAA	PCR 1, first-round PCR
o*Afpes3*-4	R	CAGTGCTATGTTCCGCCAC	*pes3* 5′DIG probe
o*Afpes3*-3	F	TTGGAGATGCGGTACTCG	
o*Afpes3*-2	R	AAGCTGCGCTTCAACCTC	PCR 2, first-round PCR
o*Afpes3*-5[b]	F	GGAACCGATCACTCAAGAC	
optrA-2	R	CATCGTGACCAGTGGTAC	PCR 3, second-round PCR
optrA-1	F	GAGGACCTGGACAAGTAC	
o*Afpes3*-6[b]	R	CGACGTAGATGAGCGATC	PCR 4, second-round PCR
o*Afpes3*-5[b]	F	GGAACCGATCACTCAAGAC	
*Afpes3*Comp1	R	CCAGAGATCGGCTAAGTGTCA	*pes3* Comp 5′
*Afpes3*Comp2	F	CGGAGGTTTTATTAGACGCCTG	
o*Afpes3*-6[b]	R	CGACGTAGATGAGCGATC	*pes3* Comp 3′
*Pes3*RT-F	F	CTCTGGCACTCCTCCAAGTC	
*Pes3*RT-R	R	AGCAATCTATCCCACGGATG	*pes3* RT-PCR
o*Afpes3*-5[b]	F	GGAACCGATCACTCAAGAC	
o*Afpes3*-6[b]	R	CGACGTAGATGAGCGATC	3.7-kb *pes3* replacement construct
calm F	F	CCGAGTACAAGGAAGCTTTCTC	*calm* RT-PCR
calm R	R	GAATCATCTCGTCGATTCGTCGTCTCAGT	

[a] F, forward; R, reverse.
[b] Some primers were used for multiple purposes as indicated.

(64). Plugs (0.6 cm^2) were taken from petri dish cultures and extracted with either 1 ml of methanol-dichloromethane-ethyl acetate (1:2:3 [vol/vol/vol]) or 1 ml of 25% (vol/vol) CH_3CN in water. These extracts were evaporated, and the residues were redissolved in 400 μl of methanol and stored at −20°C until analysis. Ultra-high-performance liquid chromatography-diode array detection (uHPLC-DAD) analyses were performed on a Dionex RSLC Ultimate 3000 (Dionex, Sunnyvale, CA). Separation was obtained on a Kinetex C_{18} column (150 by 2.1 mm, 2.6 μm; Phenomenex, Torrance, CA) maintained at 60°C using a linear gradient starting from 15% (vol/vol) CH_3CN in water (containing 50 ppm of trifluoroacetic acid) increasing to 100% (vol/vol) CH_3CN over 7 min at a flow rate of 0.8 ml/min. The injection volume was 1 μl. LC-DAD-mass spectrometry (MS) analysis was performed on an LCT oaTOF mass spectrometer (Micromass, Manchester, United Kingdom) as described by Nielsen et al. (47, 48). Chromatography was performed on a 5 cm, 3 μm, Luna C_{18} column (Phenomenex) (2) using a water-acetonitrile gradient from 15% (vol/vol) CH_3CN to 100% (vol/vol) CH_3CN in 20 min, with both solvents containing 20 mM formic acid.

Phenotypic analysis of *A. fumigatus* Δ*pes3*. For plate assays, conidia were harvested aseptically from 1-week-old malt extract agar plates and filtered through sterile Miracloth (Calbiochem) to remove mycelial matter. Conidia (10^4) were spotted onto a variety of test plates as shown in Table 4. Plates were incubated at 37°C unless otherwise stated. Colony diameter was measured periodically, and statistical analysis was carried out using two-way analysis of variance.

Vegetative growth curves were performed according to the method of Reeves et al. (56). Freshly harvested conidia were used to inoculate AMM cultures (10^7 conidia/100 ml). Cultures were incubated for 24, 48, 72, or 96 h, and the mycelial biomass was collected. Mycelia were washed in sterile water and freeze-dried to remove all liquid. Dry weights were recorded, and statistical analysis was performed using a Student *t* test.

To determine germination rates, under shaking and static conditions, AMM cultures (10 ml) were inoculated with *A. fumigatus* conidia (10^7/ml) and incubated for at least 3 h to allow germination to commence. Subsequently, 500 μl of each culture was transferred into a 2-ml screw-cap tube containing a 0.2-ml scoop of 0.1-mm glass beads, and the tubes were vortexed for 10 s. To quantify germination, 10 μl of each specimen was placed on a hemocytometer, and conidia and germlings were counted up to 100 in total. Swollen conidia were not counted as germinated. Each specimen was counted in duplicate, and the assay was performed in triplicate. Germination was recorded every hour until germination rates became constant for all strains tested. Voriconazole (VFEND; Pfizer) MIC analysis was carried out according to EUCAST guidelines (54).

TABLE 3. Restriction mapping expected fragments

DNA type	Fragment sizes (bp)
Wild-type genomic DNA	1,197, 1,053, 694, 569, 224
Δ*pes3* genomic DNA	2,197, 1,170, 694, 224
Complemented *pes3* strain (*pes3*^{C})	1,197, 1,053, 694, 569, 224

***Galleria mellonella* infection experiments.** *G. mellonella* larvae (n = 20) were inoculated into the hind proleg with 10^7 *A. fumigatus* conidia in 20 μl (per larva) as previously described (56). Mortality, defined by lack of movement in response to stimulation and discoloration (melanization) of the cuticle, was recorded at 72 h postinjection. Kaplan-Meier survival curves were analyzed by using a log-rank (Mantel-Cox) test for significance.

Murine infection experiments. Outbred male mice (strain CD1, 20 to 28 g; Charles Rivers Breeders) were used for murine virulence analyses. For analysis of the fungal burden in neutropenic mice, Immunosuppression was carried out by subcutaneous injection of 112 mg of hydrocortisone acetate/kg on day −1 and by intraperitoneal injection of 150 mg of cyclophosphamide/kg on days −3, −1, and 2. For analysis of the fungal burden in corticosteroid-treated animals immunosuppression was induced with subcutaneous injections of hydrocortisone acetate (112 mg/kg on days −3, −1, and 2). On day 0, inocula containing 7.5×10^5 or 1.5×10^6 conidia were prepared for neutropenic and corticosteroid-treated animals, respectively, in 40 μl of saline. Spores were cultured on slants of solid ACM complete medium for 5 days at 37°C prior to harvest. Spores were filtered through Miracloth and washed twice with saline prior to enumeration. Mice were anesthetized by inhalation of isoflurane and infected by intranasal instillation. Bacterial infections were prevented by adding 1 g of tetracycline/liter and 64 mg of ciprofloxicin/liter to drinking water. The weights of the infected mice were monitored for 4 days, twice daily, before the animals were culled. An *A. fumigatus para*-aminobenzoic (PABA) acid auxotroph (referred to as *A. fumigatus* H515) that is unable to germinate in the murine lung (8) was used as a positive control for attenuated virulence. For histological analyses of ATCC 46645 and Δ*pes3* infections, corticosteroid-treated animals were immunosuppressed and infected with 10^7 spores as described above. The animals were sacrificed at 14 and 24 h postinfection, and the lungs were fixed in 4% (vol/vol) formalin prior to paraffin embedding. Lung sections (n = 4) were obtained at four independent vertical sectioning levels per sample and stained with Grocotts methanamine silver (GMS) for visualization of fungal elements and with hematoxylin and eosin (H&E) for visualization of the host cells.

Measurement of the fungal burden in murine lungs. In order to assess fungal burden as a quantitative virulence criterion, quantitative PCR was performed on total genomic DNA extracted from homogenized whole lungs. The fungal burden was assessed by quantitative PCR amplification using the oligonucleotides BT-F (GAGCCCTTTTCCGACCTGAT) and BT-R (GGAACTCCTCCCGGATCTTG) to amplify the β-tubulin (AFUA_7G00250) locus from the *A. fumigatus* genome, and the oligonucleotides Actin-F (CGAGCACAGCTTCTTTGCAG) and Actin-R (C CCATGGTGTCCGTTCTGA) were used to amplify the murine actin locus (NM_007393). Quantification of both gene targets was performed in triplicate on groups of four to five mice. A modified mathematical model (incorporating adjustment for fungal inoculum) for relative quantification of the *A. fumigatus* actin and murine β-tubulin was adopted for each mouse sample using the formula ratio (R) = $(E_{\text{target}})^{\Delta CT(\text{fungal actin} - \text{murine tubulin})}$, where E is the efficiency of amplification of

TABLE 4. Phenotypic plate assay agents and observations[a]

Phenotypic test	Reagent(s) used	Concn(s) tested	Phenotype
Role of *pes3* in siderophore biosynthesis	Iron stresses (low, high, and no iron)	10 μM, 1.5 mM, and 200 μM BPS	N
Oxidative stress	Menadione	20, 30, 40 μM	N
	Diamide	0.1, 0.2, 0.4, 1, and 2 mM	Y (Δ*pes3* more resistant to diamide [0.1 mM, $P < 0.05$] than the wild type)
	Hydrogen peroxide	1, 2, and 3 mM	N
Antifungal susceptibility	Voriconazole	0.25, 0.5, 0.75, and 1.0 μg/ml	Y (Δ*pes3* more sensitive to voriconazole [0.5 μg/ml, $P < 0.001$] than the wild type)
	Amphotericin B	0.125, 0.25, 0.5, and 1.0 μg/ml	N
	Caspofungin	0.2, 0.5, and 1.0 μg/ml	N
Cell wall stress	Caffeine	2 and 5 mM	N
	Congo red	5, 10, and 15 μg/ml	N
	Calcofluor white	100 and 200 μg/ml	N
	High temp (48°C)	NA	N
Membrane stress	SDS	0.01 and 0.02% (wt/vol)	N

[a] BPS, bathophenanthroline sulfonate; SDS, sodium dodecyl sulfate; NA, not applicable; Y, yes; N, no.

target gene and is equal to 2, based on the mean of eight independent murine infections (53). The R values were $\log_{10}$ transformed and corrected for inoculum size, and reciprocal values were plotted ($1/\log_{10} R_C$). The statistical significance of variances between fungal burdens was calculated by using a nonparametric Mann-Whitney t test. Genomic DNA, isolated from animals infected with attenuated *A. fumigatus* H515 (8), was used as a positive control for attenuation.

Fungal stimulation of BMMϕ. Immortalized murine bone marrow-derived macrophages (BMMϕ) (62) were cultured in Dulbecco modified Eagle medium (Gibco) supplemented with 10% (vol/vol) fetal calf serum 1% (wt/vol) penicillin-streptomycin, and 0.5 ml of gentamicin solution. Cells were cultured in T175 flasks at 37°C with 5% CO_2. For stimulation with *A. fumigatus*, BMMϕ were washed in phosphate-buffered saline (PBS), counted, seeded onto 24-well plates containing Opti-MEM at a cell density of 10^6 cells per well, and left to adhere to 24-well plates overnight. *A. fumigatus* conidia (10^7) or germlings (5×10^6) were added to BMMϕ, followed by incubation for 18 h at 37°C. Supernatants were subsequently collected for cytokine determination by enzyme-linked immunosorbent assay (ELISA). Germling formation was achieved as described above. Preparatory experiments indicated that between 90 and 100% of conidia had formed dichotomous germ tubes after 9 h of incubation. BMMϕ were also exposed to filter sterilized culture supernatant (600 μl) from *A. fumigatus* strains. Aliquots of filter-sterilized *Aspergillus* culture supernatant were inoculated onto malt extract agar, and lack of fungal growth after 72 h confirmed that the supernatant was completely cell-free. Commercially available ELISA systems for tumor necrosis factor alpha (TNF-α), interleukin-6 (IL-6), IL-10, and RANTES determination (Peprotech UK) were used according to the manufacturer's instructions.

SEM. Dormant conidia and germlings (9 h) were Miracloth filtered and fixed using formaldehyde and glutaraldehyde in 100 mM sodium phosphate (pH 7.0) at room temperature (2 h) and 4°C (16 h). After being washed in 50 mM NH_4Cl and deionized water, the specimens were analyzed by scanning electron microscopy (SEM) by commercial arrangement (CMA, Trinity College Dublin, Dublin, Ireland).

Confocal microscopy. Germlings (9 h) were fixed with 4% (vol/vol) formaldehyde prior to two washes with PBS and blocking with bovine serum albumin (BSA; 50 mg/ml) in PBS. Incubation with murine monoclonal antibody to linear-(1,3)-β-glucan (Biosupplies; 1 μg/ml) for 1 h followed (13). The specimens were then washed twice with BSA (50 mg/ml) in PBS prior to staining with Alexa Fluor 488 goat anti-mouse IgG (H+L; Invitrogen) at 1/200 for 1 h. Germlings were washed twice with BSA (50 mg/ml) in PBS before image acquisition using an Olympus FluoView 1000 confocal microscope. Images were processed with FV10-ASW Software (v.01.07).

2D-PAGE and protein MS. *A. fumigatus* ATCC 46645 and Δ*pes3* germlings (9 h) were harvested, washed, and disrupted in lysis buffer (1 ml/g germlings) (12) using bead beating (30 Hz; three times for 5 min each time on ice) in the presence of glass beads (0.4 g; 0.1 mm), followed by centrifugation (13,000 × g, 10 min), two-dimensional polyacrylamide gel electrophoresis (2D-PAGE) fractionation (pH 4 to 7 Immobiline dry strips), and image analysis using Progenesis software (Nonlinear Dynamics, Newcastle upon Tyne, United Kingdom). Protein identification was carried out using a model 6340 ion trap LC mass spectrometer (Agilent Technologies, Santa Clara, CA) in which peptide separation was achieved by using a Nanoflow Agilent 1200 LC system and proteins were identified using Mascot MS/MS ion search (Matrix Science, London, United Kingdom).

RESULTS

Disruption and complementation of *pes3* in *A. fumigatus*. In order to gain insight into the biological role of Pes3, a *pes3* mutant strain (Δ*pes3*) was generated by homologous recombination by using the bipartite marker technique (49). Southern blot analysis was used to identify *pes3* (negative) and *ptrA* (positive) colonies by probing for a 1,568-bp EcoRI restriction fragment in the Δ*pes3* strain and a 4,139-bp fragment in the wild-type strain (Fig. 1A). Southern analysis of 14 isolates confirmed the disruption of *pes3*, and one representative clone was selected for further analysis. A complemented strain, $pes3^C$, was generated by cotransformation of *A. fumigatus* Δ*pes3* with bipartite *pes3* fragments and plasmid Pan8.1 using selection on phleomycin-containing media (Fig. 1B). Southern blot analysis of the complemented strains ($pes3^C$) produced the expected wild-type 4,139-bp fragment due to restoration of the *pes3* locus (Fig. 1A and B). Restriction mapping of part of the *pes3* locus also confirmed the integrity of the *pes3* locus following complementation (Fig. 1C). Two complemented strains ($pes3^C$), termed $pes3^{C1}$ and $pes3^{C2}$, exhibited wild-type features in all subsequent experiments. RT-PCR and real-time PCR confirmed that *pes3* transcripts were absent in the Δ*pes3* strain but present in wild-type and $pes3^C$ strains (Fig. 2). The culture conditions used for *pes3* expression analysis were as described previously by Cramer et al. (16). *pes3* transcripts were detected in wild-type and $pes3^C$ strains, but not in Δ*pes3* cultures, following 48 h of growth in RPMI medium (Fig. 2). The resulting set of strains was subjected to phenotypic analysis under various growth conditions (Table 4).

Phenotypic analysis of *A. fumigatus* Δ*pes3* reveals voriconazole susceptibility and diamide resistance. Antifungal suscep-

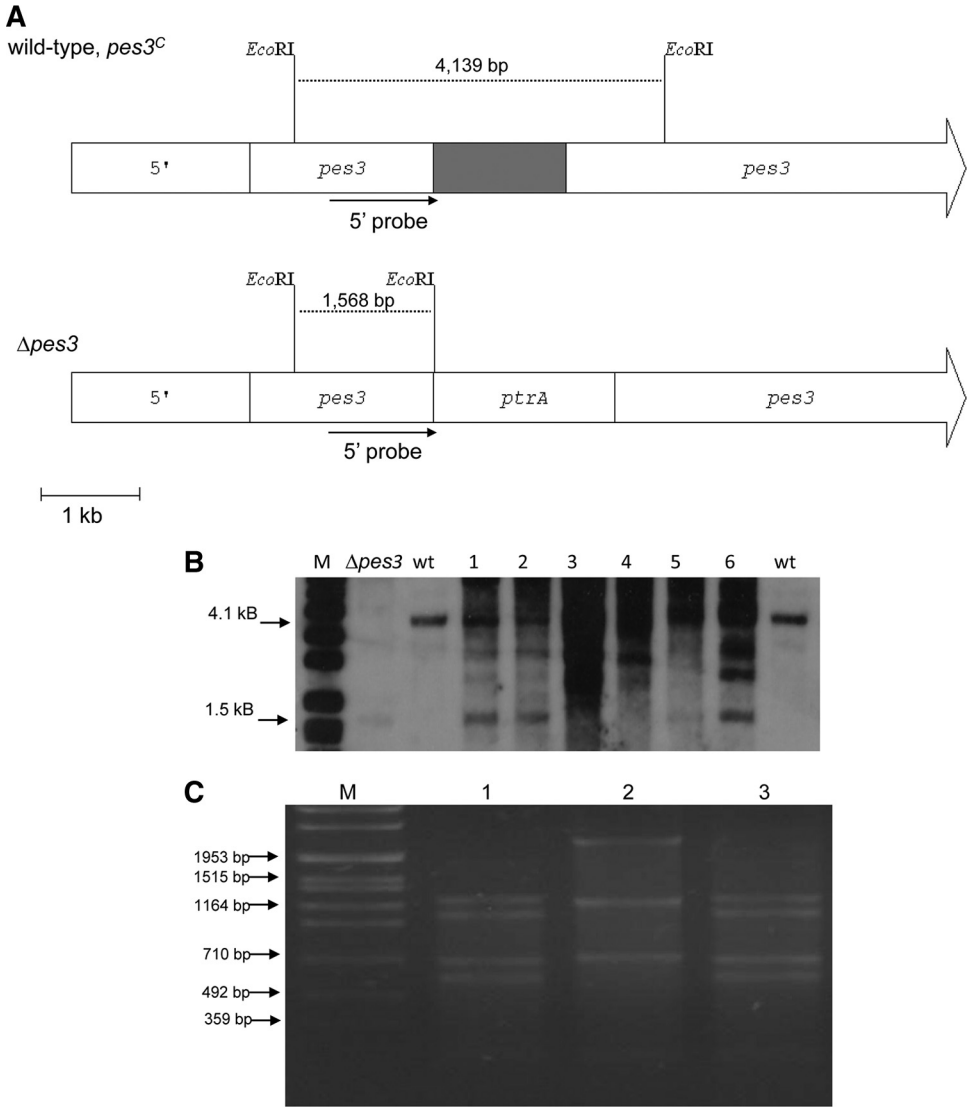

FIG. 1. Disruption and complementation of *A. fumigatus pes3*. (A) Schematic representation of Southern blot and probe hybridization, displaying the *pes3* loci in *A. fumigatus* wild-type, Δ*pes3*, and *pes3*^{C} strains. A 1.5-kb region close to the 5′ end of *pes3* (gray) was deleted and replaced by *ptrA* as indicated. EcoRI-restricted DNA was probed with a digoxigenin (DIG)-labeled probe corresponding to a region at the 5′ end of *pes3*, leading to fragments of 4,139 bp in wild-type DNA and 1,568 bp in Δ*pes3* DNA, respectively. Probe hybridization region is indicated as black lines. The full *pes3* coding sequence is 25.5 kb in length. For clarity, only a portion of *pes3* is shown here, indicated by continuous arrows. (B) Southern blot analysis of *A. fumigatus* wild-type, Δ*pes3*, and *pes3*^{C} strains confirms *pes3* disruption and subsequent complementation in *A. fumigatus* by the presence of the expected hybridization patterns as described in panel A. M, DIG-labeled marker VII (Roche); Δ*pes3*, *A. fumigatus* Δ*pes3*; wt, *A. fumigatus* wild type; lanes 3 and 4, *pes3*^{C1} and *pes3*^{C2}. Loss of the Δ*pes3* fragment (1.5 kb) in lanes 3 and 4 indicates complementation of *pes3*. (C) AgeI restriction mapping of the region with *pes3* deleted yields the expected restriction pattern (Table 3), confirming the integrity of *pes3* locus following complementation. M, Roche VII marker; lanes 1 to 3, AgeI-digested PCR products (lane 1, *A. fumigatus* wild type; lane 2, Δ*pes3*, lane 3, *pes3*^{C1}).

tibility testing indicated that strain Δ*pes3* exhibited increased susceptibility to the azole, voriconazole. The addition of voriconazole (0.25 to 1.0 μg/ml) led to a significantly reduced growth phenotype of *A. fumigatus* Δ*pes3* compared to wild-type *A. fumigatus*, and growth was restored in *pes3*^{C}. This increased sensitivity of Δ*pes3* toward voriconazole was most significant at 0.5 μg of voriconazole/ml at 62 and 72 h postinoculation ($P < 0.001$) (Fig. 3A). The MICs of voriconazole were 0.125 and 0.0625 μg/ml for the *A. fumigatus* ATCC 46645 and Δ*pes3* strains, respectively. *A. fumigatus* Δ*pes3* grew at a rate identical to that of the wild type upon exposure to other antifungal agents (amphotericin B and caspofungin). With the exception of enhanced resistance to diamide ($P < 0.05$), *A. fumigatus* Δ*pes3* grew at a rate identical to that of the wild type under all other conditions tested (Table 4).

With the observation that *pes3* transcripts were most abundant in ungerminated spores (16), germination and vegetative growth rates were compared for *A. fumigatus* wild-type and Δ*pes3* strains. Overall, *A. fumigatus* wild type and Δ*pes3* exhibited similar growth rates under shaking conditions (Fig. 3B).

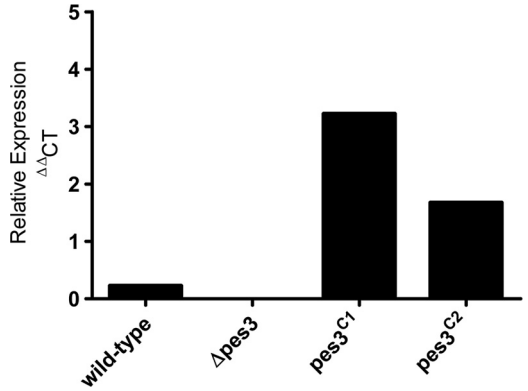

FIG. 2. Real-time PCR analysis of *pes3* expression. *A. fumigatus* wild-type, Δ*pes3*, *pes3*^{C1}, and *pes3*^{C2} strains were cultured for 48 h in RPMI medium, and real-time PCR analysis was undertaken on resultant cDNA samples. The relative abundances of *pes3* and a housekeeping gene (*calm*) transcripts are given. The lack of *pes3* expression (Δ*pes3*) and the restoration of *pes3* expression (*pes3*^{C1} and *pes3*^{C2}) can be observed. The means of three replicate PCRs for each strain are shown.

Conidial germination for both strains commenced after 3 h growth in liquid AMM, with ca. 5% germination for both strains by 5 h. By 6 h, germination had commenced for ca. 25 and 35% of the wild-type and Δ*pes3* conidia, respectively. Germination of *A. fumigatus* Δ*pes3* was significantly impeded under static conditions at 8 and 10 h, respectively ($P < 0.01$); moreover, only 10 to 20% of the conidia had germinated by 10 h (Fig. 3C). Vegetative growth determination by measuring the dry weights of the mycelial biomass for *A. fumigatus* wild-type and Δ*pes3* strains over a 96-h period indicated that both strains exhibited similar growth rates, with the exponential growth phase lasting until 48 h, and the growth rates remained stationary after this point (Fig. 3D).

***pes3* does not encode a secreted peptide.** Availability of the *A. fumigatus* Δ*pes3* mutant facilitated comparative metabolite analysis to identify a Pes3-encoded NRP. To this end, *A. fumigatus* wild-type and Δ*pes3* were cultivated in a variety of conditions, including all conditions (Table 5) under which *pes3* expression was detected. Comparative metabolite analysis, via LC-MS, of extracts from *A. fumigatus* wild-type and Δ*pes3* strains were identical and showed that there were no differences in the types or extents of metabolite production between both strains (Fig. 4). The fact that no products and/or peaks were missing in mutant samples, when analyzed using electrospray in the positive mode during MS, strongly indicates that *pes3* is not responsible for the synthesis of a soluble NRP that is secreted by, or stored intracellularly within, *A. fumigatus*, since such a product should easily be protonated and thereby detected.

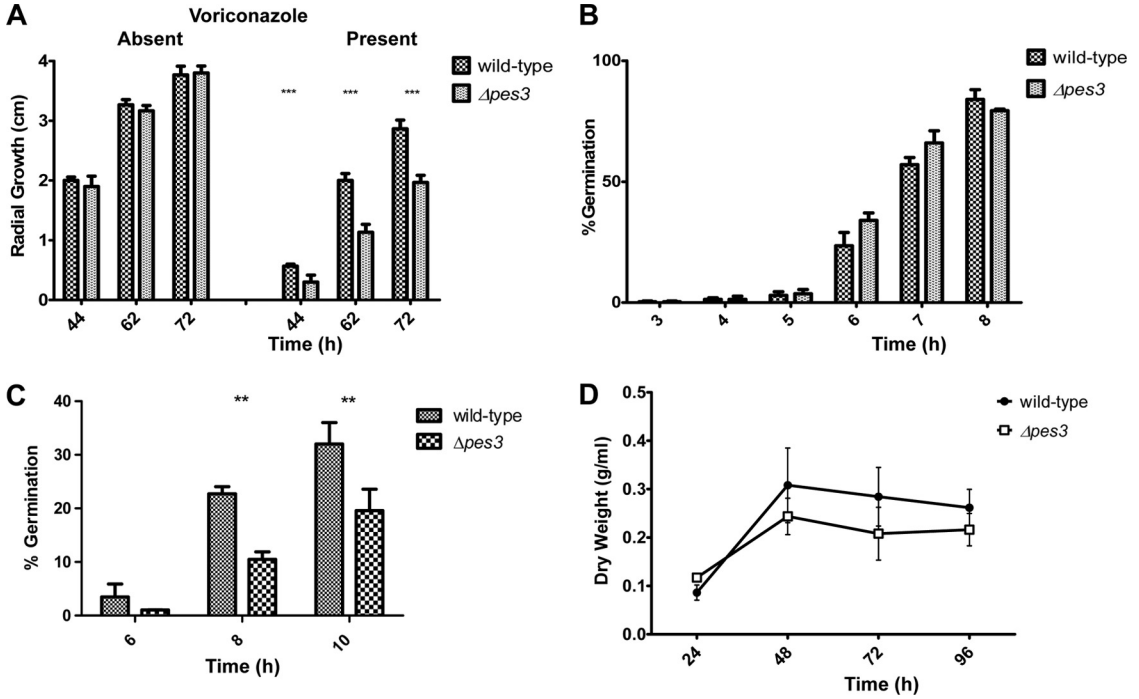

FIG. 3. *A. fumigatus* Δ*pes3* is more sensitive to voriconazole compared to the wild type, but the growth rate is not affected in *A. fumigatus* Δ*pes3*. (A) Conidia (10^4) of *A. fumigatus* wild-type and Δ*pes3* strains were spotted onto AMM plates in the presence or absence of voriconazole (0.25 to 1.0 μg/ml). Colony diameter was measured after 72 h of incubation at 37°C. The means ± the standard errors of three determinations are shown. ***, $P < 0.001$. (B) Germination rate analysis of *A. fumigatus* wild-type and Δ*pes3* strains indicates that both of them germinate at the same rate. Germination was first recorded in both strains at 3 h, and by 9 h ca. 90% of the conidia in both strains had germinated. The means ± the standard errors of three determinations are shown. (C) Analysis under static conditions confirmed that *A. fumigatus* Δ*pes3* germinates significantly slower than does the wild type ($P < 0.01$). Germination was first recorded in both strains at 6 h, and by 8 to 10 h only 10 to 20% of the mutant conidia had germinated. The means ± the standard errors of three determinations are shown. (D) Vegetative growth rates of *A. fumigatus* wild-type and Δ*pes3* strains over 96 h. No significant differences were observed between strains. The means ± the standard errors of three experiments are shown.

TABLE 5. Conditions used for comparative metabolite analysis

Condition	Description (all at 37°C)	Extraction solvent
A	RPMI liquid, 48 h of incubation	(i) Organic extraction of culture supernatant (SN) with SN-chloroform in a 1:1 ratio
B	Czapek liquid, 48 h of incubation	(ii) Neat culture supernatant injection
C	AMM liquid, 48 h of incubation	
D	Incubation on AMM agar for 6 days	Conidial extraction method (44)
E	Incubation on AMM supplemented with H_2O_2 (final concn, 2 mM) for 6 days	
F	Incubation on AMM agar for 6 days	Plug extraction method (64) using either 1 ml of methanol-dichloromethane-ethyl acetate (1:2:3 [vol/vol/vol]) or 1 ml of 25% (vol/vol) CH_3CN in water
G	Incubation on Czapek agar for 6 days	

Disruption of *pes3* leads to increased virulence in *G. mellonella* and a murine model of pulmonary aspergillosis. *G. mellonella* larvae infected with *A. fumigatus* wild type exhibited significantly lower mortality compared to those infected with *A. fumigatus* Δ*pes3* ($P < 0.001$), thereby revealing heightened virulence of the mutant strain. The percent larval survival is shown in Fig. 5. At 24 h after infection, ca. 95% of the larvae infected with the wild-type strain remained alive, whereas an 85% survival rate was observed for those infected with *A. fumigatus* Δ*pes3*, indicating increased mortality associated with *A. fumigatus* Δ*pes3*. At 48 h postinfection, 55% of the larvae infected with the wild type remained alive, in contrast to only 30% of larvae infected with Δ*pes3*. By 72 h, only 3% of larvae infected with Δ*pes3* were viable versus 23% in the wild-type group. Larval survival levels associated with *A. fumigatus* wild-type were restored in both complemented strains (*pes3*^{C1} and *pes3*^{C2}), and the overall differences in survival proportions between larvae infected with *A. fumigatus* wild type or Δ*pes3* is highly significant ($P < 0.001$).

Two murine models of pulmonary aspergillosis were used to assess the comparative virulence of the *A. fumigatus* wild-type and Δ*pes3* strains by analysis of the fungal burden. Groups of five corticosteroid-treated or neutropenic animals were infected with 7.5×10^5 or 1.5×10^6 conidia, respectively. Comparative survival (*A. fumigatus* ATCC 46645 versus Δ*pes3*) was assessed in a total of 10 mice for each strain (in two independent experiments). Although there was a tendency toward increased virulence of *A.*

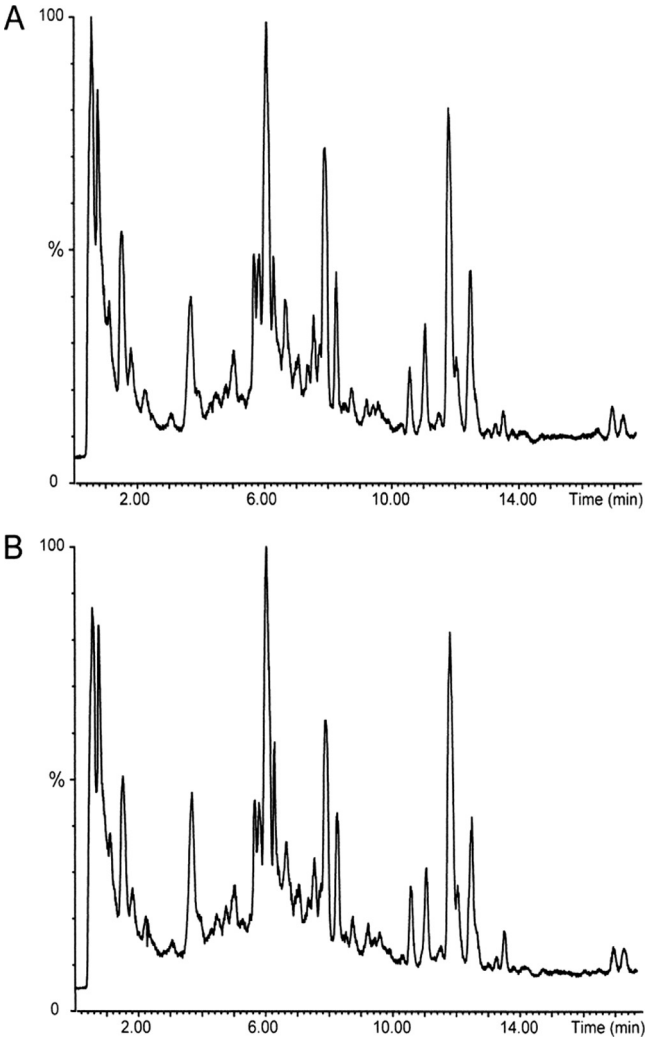

FIG. 4. *A. fumigatus* wild-type and Δ*pes3* strains exhibit identical metabolite profiles, indicating that Pes3 does not encode a secreted peptide. Total ion chromatograms (0 to 15 min) representative of metabolites detected from *A. fumigatus* wild-type (A) and Δ*pes3* (B) strains after 6 days of growth on Czapek agar. Metabolites were extracted according to condition G (see Table 5) with 1 ml of 25% (vol/vol) CH_3CN in water.

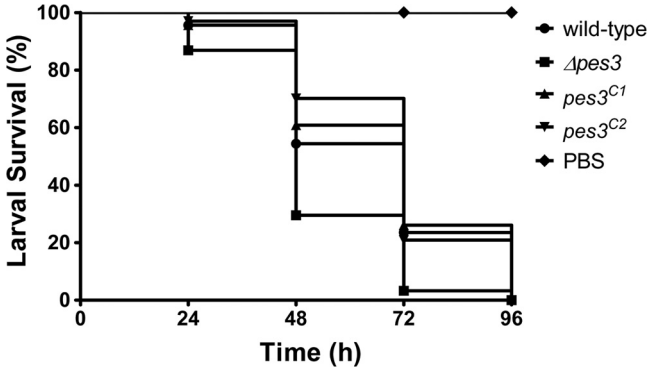

FIG. 5. Disruption of *A. fumigatus* Δ*pes3* leads to hypervirulence in an invertebrate model of invasive aspergillosis. The survival proportions of larvae ($n = 20$) infected with *A. fumigatus* wild-type, Δ*pes3*, and *pes3*^{c} strains are shown. Larval viability (%) was assessed at 24-h intervals after infection. *A. fumigatus* Δ*pes3* is more virulent than the wild type and is associated with reduced larval survival ($P < 0.001$) at all time points. Virulence is restored to wild-type levels in the two complemented strains (*pes3*^{C1} and *pes3*^{C1}). PBS was used as an injection control, and all larvae in this group remained viable for the entire experiment.

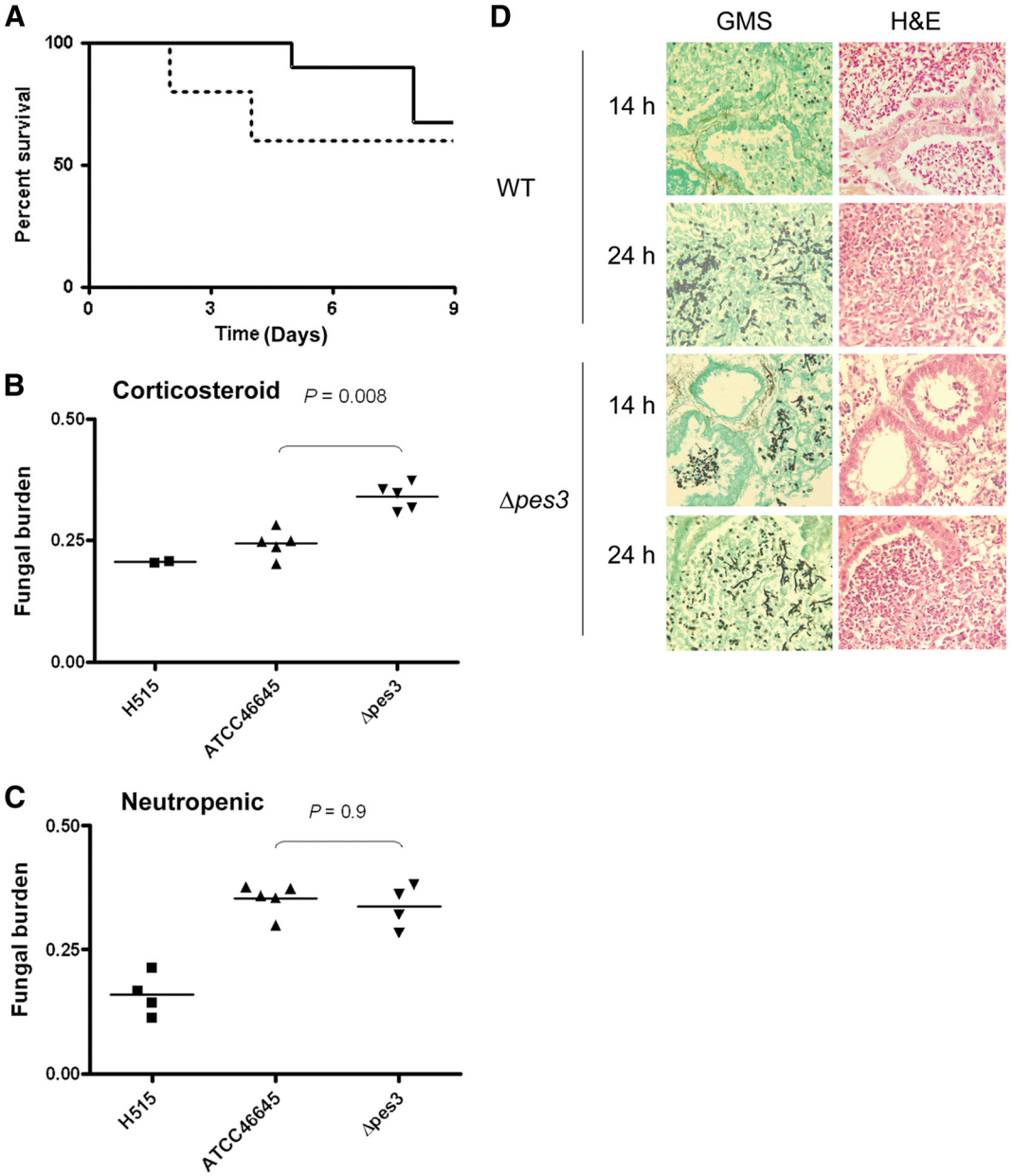

FIG. 6. Analysis of murine pulmonary aspergillosis after infection with *A. fumigatus* wild-type and Δ*pes3* conidia. (A) Survival of corticosteroid-treated mice ($n = 10$ per group) after infection with 10^6 *A. fumigatus* wild-type (solid line) or Δ*pes3* (dotted line) spores. (B and C) Fungal burden analysis corticosteroid (B) and neutropenic (C) models of pulmonary aspergillosis indicate a significantly heightened fungal burden in Δ*pes3*-infected corticosteroid treated mice. The lungs of animals infected with Δ*pes3* exhibited greater fungal burden as observed by a lower threshold cycle (C_T) value for *A. fumigatus* Δ*pes3* ($P = 0.008$). The fungal burden was quantified, relative to murine β-tubulin, by quantitative PCR using genomic DNA isolated from whole, homogenized murine lungs harvested from animals sacrificed on day 5. An attenuated *p*-amino benzoic acid auxotroph, H515 (8), was included as a control for attenuation. (D) Histological analysis of wild type- and Δ*pes3*-infected mice demonstrates rapid germination of Δ*pes3* spores in the lungs of corticosteroid-treated animals. Animals were sacrificed at 14 and 24 h postinfection, and the lungs were fixed in 4% formalin prior to paraffin embedding. Lung sections ($n = 4$) were obtained at four independent vertical sectioning levels per sample and stained with GMS for visualization of the fungal elements and with H&E for visualization of the host cells.

fumigatus Δ*pes3*, the effect was not significant as determined by log-rank analysis ($P = 0.32$) (Fig. 6A). However, corticosteroid-treated animals infected with Δ*pes3* demonstrated a rapid decline in weight relative to the day of infection; every animal infected with *A. fumigatus* Δ*pes3* exhibited weight loss over the course of the infection. Two *A. fumigatus* Δ*pes3*-infected animals exhibited >20% weight loss by day 4 of the experiment, whereas animals infected with *A. fumigatus* wild type displayed moderate fluctuations in weight during infection, but none dropped below 20% of starting weight (see Fig. S1 in the supplemental material). The mean weights of animals at day 5 of the infection were significantly lower for the *A. fumigatus* Δ*pes3* infection group (93.00 ± 2.5% of the starting weight) than the wild-type counterpart (106.2% ± 1.62% of the starting weight) ($P < 0.01$) (see Fig. S1

in the supplemental material). Animals in the *A. fumigatus* H515 control group remained at a steady weight over the course of the experiment (see Fig. S1 in the supplemental material). The fungal burden was quantified, relative to murine β-tubulin, by quantitative PCR using genomic DNA isolated from whole, homogenized murine lung harvested from animals sacrificed on day 5. An attenuated *p*-amino benzoic acid auxotroph, H515 (8), was included as a control for attenuation. Infection of hydrocortisone acetate-treated animals with strain Δ*pes3* resulted in significantly heightened fungal burden (Fig. 6B, $P = 0.008$) relative to infection with ATCC 46645. In contrast, the fungal burdens following infection of neutropenic mice with Δ*pes3* and ATCC 46645 were comparable (Fig. 6C, $P = 0.9$).

In order to determine the basis of increased fungal burden in Δ*pes3*-infected animals, we studied the histological progression of aspergillosis in the lungs of corticosteroid-treated animals at 14 and 24 h postinfection (Fig. 6D). The major difference between wild-type and Δ*pes3* infections was earlier germination of the Δ*pes3* spores. At 14 h postinfection, the majority of Δ*pes3* spores had germinated and produced germ tubes. Germinating spores were observable in the lung alveoli and in the bronchioles, and inflammatory cell infiltrates were observed in regions of spore deposition (Fig. 6D). In contrast, lungs infected with the wild-type isolate exclusively harbored ungerminated spores at 14 h postinfection. Large regions of inflammatory infiltration were observable in which the ultrastructure of the lung tissue was barely visible and spores were distributed throughout the lung parenchyma, including within the bronchioles that were heavily infiltrated with inflammatory cells. At 24 h postinfection, the observed disparate germination was limited to areas of high inflammation. Although a trend toward lessened inflammation in Δ*pes3*-infected lungs was clearly discernible, the difference between wild type- and Δ*pes3*-infected lungs was not dramatic, and quantitation of the difference was therefore not attempted from the lung sections. In summary, the heightened virulent phenotype observed for Δ*pes3* in the hydrocortisone acetate model is associated with a reduction in weight loss and an increase in fungal burden in the murine lung.

***A. fumigatus* Δ*pes3* exhibits an immunologically silent phenotype compared to the wild type.** In order to test the hypothesis that increased virulence of *A. fumigatus* Δ*pes3* in both insect and murine models could be due to immunological silencing and a consequent attenuated immune response, we monitored cytokine production following coincubation of BMMϕ with *A. fumigatus* 9-h germlings. This analysis revealed a reduction in four cytokines TNF-α (30% reduction; 2,592 ± 290 versus 3,686 ± 1,719 pg/ml [mean ± the standard deviation]), IL-6 (68% reduction), RANTES (25% reduction), and IL-10 (10% reduction) after coincubation of BMMϕ with *A. fumigatus* Δ*pes3* compared to coincubation of BMMϕ with the wild type (Fig. 7; see Fig. S2 in the supplemental material). The level of TNF-α produced in response to Δ*pes3* germlings resembled that of the response toward *A. fumigatus* conidia, either live or dead (2,000 to 2,500 pg/ml), and similar levels of TNF-α were produced in response to *A. fumigatus* wild-type and *A. fumigatus* Δ*pes3* conidia. Cytokines were not detected from BMMϕ in response to *A. fumigatus* wild-type or Δ*pes3* culture supernatants (data not shown). These data suggest that the recognition of Δ*pes3* by pattern recognition receptors

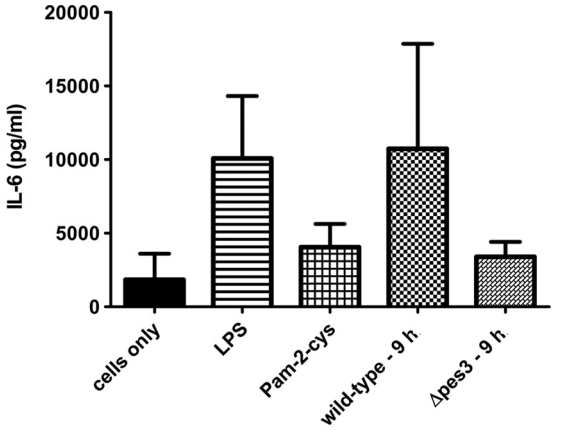

FIG. 7. Coincubation of murine macrophages with *A. fumigatus* Δ*pes3* leads to a reduction in IL-6 secretion compared to *A. fumigatus* wild type. BMMϕ were stimulated with the TLR ligands lipopolysaccharide (LPS; TLR4 ligand) and Pam-2-cys (TLR2 ligand), as well as *A. fumigatus* wild-type and Δ*pes3* germlings/conidia for 9 h. Cytokine secretion was then assessed by ELISA. Less IL-6 (68% reduction) was detected from BMMϕ after incubation with *A. fumigatus* Δ*pes3* (Δ*pes3* - 9 h) compared to wild-type germlings (wild-type - 9 h). The means ± the standard errors of two biological replicates are shown.

(PRRs) of the innate immune system may be less efficient than recognition of the wild type, leading to diminished cytokine secretion in BMMϕ upon coincubation with *A. fumigatus* Δ*pes3*, and this may, in part, explain the increased virulence and increased fungal burden compared to Δ*pes3*.

Loss of *pes3* impairs germ tube formation. SEM pretreatment resulted in visible germling aggregation for *A. fumigatus* Δ*pes3.* Comparative SEM analysis revealed impeded germination of *A. fumigatus* Δ*pes3* germlings. The hyphae of mutant germlings appeared smoother, compared to the wild type (Fig. 8A), and the rod-like strands apparent on the hyphal surface of wild-type germinating conidia were effectively absent from the shorter hyphae of *A. fumigatus* Δ*pes3*. No structural differences were apparent between ungerminated *A. fumigatus* wild-type and Δ*pes3* conidia (data not shown).

***A. fumigatus* Δ*pes3* exhibits proteome alteration.** 2D-PAGE, quantitative image analysis, and tandem MS (MS/MS) confirmed the up- and downregulation of 15 and 10 proteins, respectively, in *A. fumigatus* Δ*pes3* compared to the wild type (Table 6). Upregulated proteins (1.6- to 4.1-fold) included the Rab11 GTPase and ribosomal, heat shock, and electron transport chain proteins, while those downregulated (1.6- to 3.1-fold) included the pentafunctional polypeptide AroM (AFUA_1G13740) and spermidine synthase (AFUA_1G13490).

DISCUSSION

Sequencing of the *A. fumigatus* genome has revealed the presence of at least 14 genes encoding NRP synthetases (16, 50). However, specific data relating the majority of these NRP synthetases to an NRP product has not been forthcoming (66). The *pes3* gene was disrupted and subsequently complemented in the *A. fumigatus* ATCC 46645 strain, with the aim of elucidating the peptide encoded by Pes3, a strategy used by others to identify the peptides encoded by NRP synthetases (15, 36, 39, 60). Unlike several other fungal NRP synthetases charac-

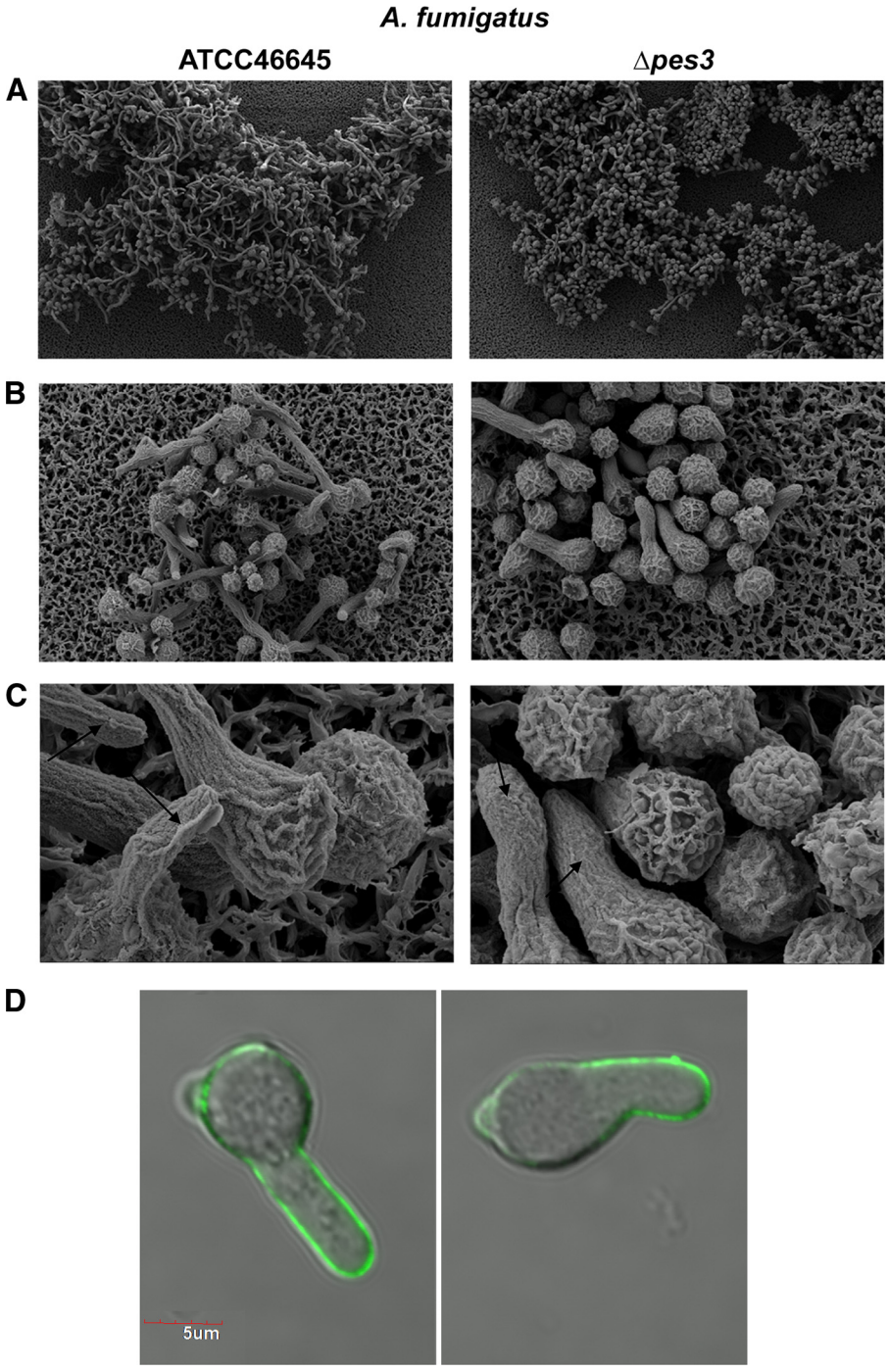

FIG. 8. SEM and confocal microscopy analysis of *A. fumigatus* ATCC 46645 and Δ*pes3* germlings (9 h). (A) *A. fumigatus* wild-type germlings exhibit longer germ tubes and undergo a higher degree of germination compared to Δ*pes3* (×500 magnification). (B) *A. fumigatus* wild-type germlings exhibit narrower germ tubes than Δ*pes3* germlings (×2,000 to ×3,000 magnification) (C) The surface appearance of *A. fumigatus* Δ*pes3* is smoother than that of the wild type and lacks distinctive rod-like strands (×10,000 magnification). (D) Surface β-glucan expression on germlings is significantly different between *A. fumigatus* wild-type and Δ*pes3* strains; less β-glucan is present on mutant germlings ($P = 0.0325$). The difference in germling length is also clearly evident.

terized to date, Pes3 is not primarily involved in the protection of *A. fumigatus* against oxidative stress and does not secrete an NRP product, as evidenced by the lack of peptide identification following exhaustive metabolite analysis. *A. fumigatus* Δ*pes3* displayed increased sensitivity toward the antifungal voriconazole compared to the wild type. *A. fumigatus* Δ*pes3* was hypervirulent in an invertebrate and showed heightened virulence in an HCA murine model of pulmonary aspergillosis, and stimulation of murine macrophages with *A. fumigatus* Δ*pes3* resulted in reduced cytokine production compared to

TABLE 6. Comparative proteomic analysis of *A. fumigatus* wild-type versus Δ*pes3* germlings

Protein	No.[a]	Annotation name	Gene identity	Fold change[b]	tpI[c]	tM_r[d]	No. of peptides matched	% Sequence coverage
Upregulated in *A. fumigatus* Δ*pes3*	328	Glycine dehydrogenase	AFUA_4G03760	1.8	6.71	116,116	11	12
	698	t-Complex protein 1, zeta subunit	AFUA_3G09590	2.2	6.31	59,081	2	6
	1108	NGG1 interacting factor Nif3	AFUA_6G12480	1.7	6.08	42,126	7	23
	1291	ATP synthase gamma chain, mitochondrial precursor	AFUA_1G03510	1.8	8.31	32,530	14	47
	1352	Glucosamine-6-phosphate deaminase	AFUA_1G00480	3.2	8.35	40,181	1	4
	1478	GTP-binding nuclear protein Ran	AFUA_6G13300	1.9			6	23
	1497	Heat shock protein 70	AFUA_1G07440	2.6	5.09	69,792	3	2
	1512	Heat shock protein Hsp30/Hsp42	AFUA_3G14540	1.6	6.09	20,450	7	46
	1534	Ubiquinol-cytochrome *c* reductase iron-sulfur subunit precursor	AFUA_5G10610	1.8	9.20	33,111	12	33
	1547	Ubiquinol-cytochrome *c* reductase iron-sulfur subunit precursor	AFUA_5G10610	2.7	9.20	33,111	1	7
	1557	Ras GTPase Rab11	AFUA_1G02190	3.6	5.95	22,568	8	43
	1562	40S ribosomal protein S5	AFUA_1G15020	3.2	9.35	25,886	1	6
	1566	Mitochondrial ATPase subunit ATP4	AFUA_8G05440	2.0	9.36	29,767	9	33
	1668	60S Ribosomal protein L5	AFUA_1G12890	4.1	8.59	35,519	3	14
	1771	Molecular chaperone Hsp70	AFUA_1G07440	2.1	5.09	69,792	4	7
	1948	Enolase/allergen AspF 22	AFUA_6G06770	2.1	5.39	47,392	16	42
Downregulated in *A. fumigatus* Δ*pes3*	128	Pentafunctional polypeptide (AroM)	AFUA_1G13740	2.9	6.15	175,521	13	12
	244	Pyruvate carboxylase	AFUA_4G07710	2.2	6.23	132,003	16	16
	576	Transketolase TktA	AFUA_1G13500	3.1	6.12	75,245	15	24
	585	Transketolase TktA	AFUA_1G13500	2.5	6.12	75,245	22	31
	714	Phosphoglucomutase	AFUA_3G03020	2.2	5.78	56,680	8	18
	1060	Actin	AFUA_6G04740	2.1	5.37	43,397	17	52
	1242	Spermidine synthase	AFUA_1G13490	1.8	NA[e]	NA	8	28
	1457	Phosphoserine phosphatase	AFUA_4G12730	1.6	5.67	33,442	6	26
	1494	Glycerol-3-phosphate phosphatase	AFUA_1G10570	2.5	5.48	25,765	7	34
	1773	Nascent polypeptide-associated complex (NAC) subunit	AFUA_6G02750	2.0	5.32	20,591	7	27
	1923	Aminopeptidase	AFUA_5G04330	2.0	6.26	109,277	16	22

[a] No., spot number following 2D-PAGE.
[b] The fold change upward is given for proteins that are upregulated in *A. fumigatus* Δ*pes3*, and the fold change downward is given for proteins that are downregulated in *A. fumigatus* Δ*pes3*.
[c] tpI, theoretical isoelectric point.
[d] tM_r, theoretical molecular weight ratio.
[e] NA, not applicable.

stimulation with the wild type. We hypothesize that this is due to a structural alteration in *A. fumigatus* Δ*pes3*, occurring in the vicinity of the cell wall which abrogates a pathogen associated molecular pattern (PAMP), thereby leading to defective recognition by innate immune receptors. With respect to the histology observed in infected animals, there are several plausible explanations for such a deficiency. Although we observed a slight reduction in inflammation associated with Δ*pes3* infection in corticosteroid-treated animals, recruitment of host inflammatory cells is evidently only marginally affected. This would imply that, rather than being "invisible" to host immunity (as, for instance, in the case of *A. fumigatus* Δ*rodA* [2]), the Δ*pes3* strain is resistant to killing by the host. This might feasibly result from either or both of (i) an altered local cytokine environment or (ii) the enhanced growth rate of Δ*pes3*, which may outgrow macrophages and thereby avoid killing or possibly only transiently display a PAMP. In any case, the lungs of mice infected with *A. fumigatus* Δ*pes3* exhibited greater fungal burden compared to mice infected with the wild type, suggesting inefficient clearance of *A. fumigatus* Δ*pes3* by the immune system. Taken together, these data indicate a structural role for an NRP synthetase product, which represents a novel finding for an NRP synthetase in *A. fumigatus*.

Since relatively little is known about the biological role of NRP synthetases in *A. fumigatus*, a starting point for investigation was to probe pathways in which fungal NRP synthetase involvement has already been demonstrated. Phenotypic analyses eliminated a role for *pes3* in siderophore biosynthesis and protection against oxidative stress, despite widely reported roles for *A. fumigatus* and other fungal NRP synthetases in these processes (36, 51, 57, 58, 60). Expression of *pes3* was detected at low levels in liquid cultures in our study, in agreement with an earlier study by Cramer et al. (16). The high level of *pes3* expression observed in ungerminated spores (16) hinted at a possible role for *pes3* in germination or cell wall structure in *A. fumigatus*. Analysis of both vegetative and germination growth rates revealed that *A. fumigatus* Δ*pes3* grew at an rate identical to that of the wild type, ruling out an essential role for *pes3* in conidial germination and mycelial growth. Exposure of *A. fumigatus* wild-type and Δ*pes3* strains to a range of cell wall-damaging agents in the present study according to a recently described protocol for identifying fungal cell wall mutants (55) revealed no altered phenotypes for Δ*pes3*, therefore eliminating a major role for *pes3* in modeling cell wall architectures affected by these agents. However, *A. fumigatus* Δ*pes3* did exhibit significantly increased sensitivity toward the antifungal voriconazole ($P < 0.001$), possibly caused by increased entry of voriconazole into conidia due to absence of the Pes3-encoded NRP. The increased voriconazole sensitivity of *A. fumigatus* Δ*pes3* may be related to the significantly reduced β-glucan presence on hyphal surfaces, if β-glucan acts to sequester antifungal drugs. Our observations are consistent

with previous work which demonstrated that antifungal drug resistance in *Candida albicans* requires extracellular (1,3)-β-glucan, which acts to sequester and prevent fluconazole uptake into the cell (46). Thus, we hypothesize that altered β-glucan presence on hyphal surfaces, consequent to *pes3* disruption, sensitizes *A. fumigatus* Δ*pes3* to voriconazole. Moreover, resistance to diamide may be due to decreased intracellular glutathione in *A. fumigatus* Δ*pes3*.

Genes encoding secondary metabolites are often organized into clusters, and at least 22 such clusters have been identified in *A. fumigatus* (28, 50, 52). A master regulator of secondary metabolism, LaeA, has been identified in *A. fumigatus* (6), and this was found to transcriptionally regulate at least 13 secondary metabolite clusters in *A. fumigatus* (6, 52). Interestingly, *pes3* was not found to be under LaeA regulation (52), which suggested it might not be responsible for the production of a secreted metabolite. Extensive comparative metabolite analysis between the wild-type and Δ*pes3* strains showed that this was in fact the case, with metabolite profiles for wild-type and Δ*pes3* identical under all of the conditions explored (Table 5). The metabolite extraction and analysis method used in the present study was sufficient to determine all known secreted secondary metabolites from 395 fungal isolates (64). Furthermore, the comparative analysis included conditions in which *pes3* expression was confirmed in the present study and others, including analysis of ungerminated spores, where *pes3* expression was most abundant (16). Taken together, these results unambiguously infer that Pes3 does not produce either a secreted or an intracellularly located metabolite in *A. fumigatus*.

NRP synthetases have been widely implicated in mediating fungal virulence. Surprisingly, *in vivo* virulence testing indicated that *A. fumigatus* Δ*pes3* exhibited increased virulence in both an invertebrate model, *G. mellonella*, and in an HCA immunosuppressed murine model of IA, demonstrating that deletion of *pes3* augments the virulence of *A. fumigatus*. In order to explain the virulence of *A. fumigatus* Δ*pes3*, several hypotheses were explored. A reduced growth rate of *A. fumigatus* Δ*pes3* compared to the wild type could result in augmented virulence of *A. fumigatus* Δ*pes3* by invoking an attenuated immune response due to reduced availability of fungal components for immune recognition. Alternatively, increased stimulation of the immune response could result from an accelerated growth rate, leading to greater inflammation, and/or greater production of toxic secondary metabolites. However, the identical growth rates observed between *A. fumigatus* wild-type and Δ*pes3* eliminate this hypothesis. Second, we found that Pes3 does not appear to encode a secreted metabolite, and the uniformity of metabolite profiles for wild-type and *A. fumigatus* Δ*pes3* makes it unlikely that an alteration in secondary metabolite biosynthesis is responsible for the increase in virulence of *A. fumigatus* Δ*pes3*. A more plausible hypothesis is that *A. fumigatus* Δ*pes3* is immunologically silenced compared to the wild type, and support for this hypothesis was obtained from immune signaling data, whereby a reduction in cytokine induction (TNF-α, IL-6, RANTES, and IL-10) was observed in murine macrophages stimulated with *A. fumigatus* Δ*pes3* compared to those stimulated with the wild type. These results indicate that the NRP encoded by Pes3 may be necessary for efficient recognition of *A. fumigatus* by the innate immune system. No increase in virulence was observed between *A. fumigatus* wild-type and Δ*pes3* in a neutropenic model of IA, with similar weights and fungal burdens in the lungs of animals ($n = 5$) infected with either wild-type or Δ*pes3*, indicating that neutrophil presence is required for the increased virulence of Δ*pes3*, and that the role played by Pes3 in immune recognition leads to an immune response mediated largely by neutrophils.

Innate recognition of fungal pathogens involves specific recognition of invariant molecular components of pathogens, known as PAMPs, by PRRs (42, 72). Dectin-1, a type II transmembrane protein that belongs to the NK-like C-type lectin-like family, is a known receptor for fungal β-glucans (7). Since the initial discovery of dectin-1, this receptor has received significant attention for its essential role in the pulmonary innate immune response against *A. fumigatus* (25, 67, 75). The role of Toll-like receptors (TLRs) in the immunological recognition of *A. fumigatus* has also been studied, with TLR2 and TLR4 being implicated (40, 43, 74, 76). Several discrepancies have been documented between the role of TLR2 and TLR4 in recognition of *A. fumigatus* and, to date, no *A. fumigatus* PAMPs that are recognized by TLRs have been described (14), highlighting the importance of this research area. In fact, with the exception of *C. albicans* phospholipomannan, the fungal ligands stimulating TLR activation remain undefined (37). It has been suggested that the ligands activating TLRs in response to *A. fumigatus* may be of carbohydrate, lipid, or protein origin (25). Given the observations made during the present study, it is likely that this is the case and that Pes3 encodes a peptide with a structural role that is necessary for the recognition of *A. fumigatus*.

There is one other report describing a fungal NRP synthetase gene that is likely to encode an NRP with a structural role. *AbNPS2* in the plant pathogen *Alternaria brassicola* was identified to encode a large multimodular NRP synthetase (29). Deletion of *AbNPS2* resulted in several altered phenotypes in the resultant mutant; reduced virulence on cabbage leaves, lower conidial germination rates, reduced hydrophobicity of conidia, and an altered conidial surface. The conidial surface in the wild type was smooth and had a compact cell wall, whereas the surfaces of *AbNPS2* mutant conidia were fluffy, and the cell wall layers were separated as determined by transmission electron microscopy (29). The authors of that study hypothesized that the *AbNPS2*-encoded peptide may be a component of, or facilitate linkage to, the outermost layer and the middle layer of the fungal conidial cell wall, a hypothesis that may also be relevant for the Pes3-encoded peptide. Dormant *A. fumigatus* conidia are covered by a hydrophobic rodlet layer (69). The rodlet layer is composed of hydrophobic proteins, and this layer maintains *A. fumigatus* conidia in an immunologically silenced state (2). Recently, it has been shown that one of the rodlet proteins, RodA, prevents *A. fumigatus* conidia from triggering NET formation by human neutrophils (9), indicating the importance of rodlet removal in leading to a neutrophil-mediated immune response. To our knowledge, the processes involved in linkage and removal of the rodlet layer to the cell wall have not yet been described, and we speculate that Pes3 may biosynthesize a peptide which is involved in removal of the rodlet layer from the surface of *A. fumigatus* conidia. Loss of a Pes3-encoded peptide could lead to incomplete or delayed removal of the rodlet layer during conidial germination, thereby maintaining *A. fumigatus* Δ*pes3* in an immunologically

silenced state, leading to the phenotypes observed here. Alternatively, Pes3 might encode a peptide that functions in linking the rodlet layer to the cell wall. Loss of Pes3 could result in aberrant linking of the rodlet layer to the cell wall and may hinder the removal of the rodlet (e.g., RodAp) layer upon germination. Either hypothesis would result in a reduction in the exposure to fungal cell wall components and explain the reduced immune recognition of and observed virulence for *A. fumigatus* Δ*pes3*. It has been proposed that RodA may be antiphagocytic, either via steric blocking and/or by impeding macrophage recognition of conidia (19).

Interestingly, the majority of *A. fumigatus* mutants for which hypervirulent phenotypes have been reported relate to a defect in the cell wall or conidial surface. For example, disruption of the glycosylphosphatidylinositol-anchored protein ECM33 resulted in hypervirulence in a murine model of IA, which was possibly due to a softer cell wall, allowing faster germination (59). Hypervirulent phenotypes were also observed following mutations in the α(1-3)-glucan synthase AGS3, the transcription factor ACE2, and the trehalose biosynthesis genes *tpsA* and *tpsB*, and in all cases defects could be detected at the cell walls of these mutants (3, 21, 41). The ACE2 mutant was hypervirulent in a non-neutropenic murine model of IA, but no difference in virulence was observed in a neutropenic model of IA (21), indicating that, as with *A. fumigatus* Δ*pes3*, the presence of neutrophils was necessary for the increased virulence of the Δ*ace2* strain. *A. fumigatus ppoA* to *ppoC* encode dioxygenases responsible for prostaglandin biosynthesis, and it has been shown that a triple *A. fumigatus ppo* mutant, generated using RNA interference, exhibited increased virulence in a murine model of invasive pulmonary aspergillosis (71). Like *A. fumigatus* Δ*pes3*, this mutant indicated few phenotypes, however a *ppoC* deletion mutant exhibited an altered conidial size and retarded germination in static cultures compared to the wild type (18). In addition, *A. fumigatus* Δ*ppoC* virulence was not significantly altered in a non-neutropenic mouse model, and yet it exhibited a greater susceptibility to macrophage killing than did the wild type. Together, these findings suggest an altered cell wall composition (18)—as we speculate for *A. fumigatus* Δ*pes3*.

Proteome alterations in *A. fumigatus* Δ*pes3* (Table 6) reveal interesting insights into Pes3-encoded peptide functionality and the interplay between membrane-endosome trafficking and morphogenesis. Rab11 (AFUA_1G02190) shares up to 75% identity with mammalian orthologs, regulates plasma membrane-endosome trafficking in *Drosophila melanogaster* (4), and is upregulated (3.6-fold) in *A. fumigatus* Δ*pes3* (Table 6). This linkage between Pes3 loss and possible perturbation in endocytic trafficking is significant in the context of increased voriconazole sensitivity of this mutant (Fig. 3 and Table 4) and suggests a role for the Pes3-encoded peptide in membrane-cell wall interactions. Elevated expression of ribosomal, heat shock, and electron transport proteins in *A. fumigatus* Δ*pes3* (Table 6) suggest generalized cell stress and an increased energy requirement and is probably a consequence of impaired conidial germination. Downregulation of protein expression in *A. fumigatus* Δ*pes3* is correspondingly illuminating: decreased actin expression (2.1-fold) in *A. fumigatus* Δ*pes3* is in accordance with impaired germ tube length. The pentafunctional AroM protein interconverts metabolites of quinic acid in the shikimate pathway, to produce aromatic amino acids, by catalyzing the conversion of 3-deoxy-D-arabinoheptulosonic acid 7-phosphate into 5-enolpyruvylshikimate 3-phosphate (23). Previous work in *A. nidulans* showed that the constitutive overexpression of AroM inhibited conidial germination (34); thus, it is plausible that AroM downregulation in *A. fumigatus* Δ*pes3* (Table 6) represents a systems strategy to overcome the attenuated conidial germination due to Pes3 absence. Spermidine synthase in *Ustilago maydis* is required for both morphogenesis (yeast-to-mycelium transition) and fungal survival during the infection of plants (73); moreover, deletion mutants were auxotrophic for both lysine and spermidine. In addition, Jin et al. (26) demonstrated that spermidine synthase deletion in *A. nidulans* caused morphological defects and altered germination, as we observed for *A. fumigatus* Δ*pes3* (Fig. 8A). Given that spermidine synthase is downregulated in *A. fumigatus* Δ*pes3*, we speculate that it may be downstream of, or affected by, Pes3 function; otherwise, increased expression would have been observed to counteract the inhibitory effects of Pes3 absence.

The exact nature of the Pes3-encoded peptide remains to be elucidated, as does that encoded by AbNPS2 (29), thereby highlighting the significant challenge that exists for relating NRP synthetases, particularly those with a structural role, to their respective NRP products. However, all of the data generated in the present study strongly suggest a structural role for the Pes3-encoded NRP in *A. fumigatus*, and elucidation of the exact nature of this peptide will be the focus of future studies. The agreement between the *G. mellonella* and the murine virulence data further consolidates the robustness of the larval model in discriminating between the virulence potential of different fungal isolates, a topic that has recently attracted much attention (27, 63).

ACKNOWLEDGMENTS

This study was supported by an Embark Ph.D. Fellowship to K.A.O. from the Irish Research Council for Science Engineering and Technology. T.C. was supported by a studentship awarded to the Section of Microbiology, Imperial College London, by the Biotechnology and Biosciences Research Council. D.S. and M.S. were recipients of HEA-PRTLI-3 funding and an EU Marie Curie Fellowship (MTKD-CT-2004-014436), respectively. Quantitative RT-PCR instrumentation was funded by Science Foundation Ireland (SFI; grant SFI/07/RFP/GEN/F571/ECO7). The LC-MS facilities were funded by the Danish Research Agency for Technology and Production (grant 09-064967) and the Irish Higher Education Authority.

We thank Ica Dix for assistance with confocal microscopy (SFI-funded instrumentation). We are also grateful to R. Cramer for very helpful advice on the germination assays.

REFERENCES

1. **Abad, A., et al.** 2010. What makes *Aspergillus fumigatus* a successful pathogen? Genes and molecules involved in invasive aspergillosis. Rev. Iberoam. Micol. **27:**155–182.
2. **Aimanianda, V., et al.** 2009. Surface hydrophobin prevents immune recognition of airborne fungal spores. Nature **460:**1117–1179.
3. **Al-Bader, N., et al.** 2010. Role of trehalose biosynthesis in *Aspergillus fumigatus* development, stress response, and virulence. Infect. Immun. **78:** 3007–3018.
4. **Assaker, G., D. Ramel, S. K. Wculek, M. González-Gaitán, and G. Emery.** 2010. Spatial restriction of receptor tyrosine kinase activity through a polarized endocytic cycle controls border cell migration. Proc. Natl. Acad. Sci. U. S. A. **107:**22558–22563.
5. **Balibar, C. J., and C. T. Walsh.** 2006. GliP, a multimodular nonribosomal peptide synthetase in *Aspergillus fumigatus*, makes the diketopiperazine scaffold of gliotoxin. Biochemistry **45:**15029–15038.

6. **Bok, J. W., and N. P. Keller.** 2004. LaeA, a regulator of secondary metabolism in *Aspergillus* spp. Eukaryot. Cell **3:**527–535.
7. **Brown, G. D., et al.** 2002. Dectin-1 is a major β-glucan receptor on macrophages. J. Exp. Med. **196:**407–412.
8. **Brown, J. S., et al.** 2000. Signature-tagged and directed mutagenesis identify PABA synthetase as essential for *Aspergillus fumigatus* pathogenicity. Mol. Microbiol. **36:**1371–1380.
9. **Bruns, S., et al.** 2010. Production of extracellular traps against *Aspergillus fumigatus* in vitro and in infected lung tissue is dependent on invading neutrophils and influenced by hydrophobin RodA. PLoS Pathog. **6:**18.
10. **Burns, C., et al.** 2005. Identification, cloning, and functional expression of three glutathione transferase genes from *Aspergillus fumigatus*. Fungal Genet. Biol. **42:**319–327.
11. **Calvo, A. M., R. A. Wilson, J. W. Bok, and N. P. Keller.** 2002. Relationship between secondary metabolism and fungal development. Microbiol. Mol. Biol. Rev. **66:**447–449.
12. **Carberry, S., C. M. Neville, K. A. Kavanagh, and S. Doyle.** 2006. Analysis of major intracellular proteins of *Aspergillus fumigatus* by MALDI mass spectrometry: identification and characterization of an elongation factor 1B protein with glutathione transferase activity. Biochem. Biophys. Res. Commun. **314:**1096–1104.
13. **Chamilos, G., et al.** 2010. Generation of IL-23 producing dendritic cells (DCs) by airborne fungi regulates fungal pathogenicity via the induction of T(H)-17 responses. PLoS One **5:**e12955.
14. **Chignard, M., V. Balloy, J. M. Sallenave, and M. Si-Tahar.** 2007. Role of Toll-like receptors in lung innate defense against invasive aspergillosis: distinct impact in immunocompetent and immunocompromised hosts. Clin. Immunol. **124:**238–243.
15. **Cramer, R. A., et al.** 2006. Disruption of a nonribosomal peptide synthetase in *Aspergillus fumigatus* eliminates gliotoxin production. Eukaryot. Cell **5:**972–980.
16. **Cramer, R. A., et al.** 2006. Phylogenomic analysis of non-ribosomal peptide synthetases in the genus *Aspergillus*. Gene **383:**24–32.
17. **Dagenais, T. R. T., and N. P. Keller.** 2009. Pathogenesis of *Aspergillus fumigatus* in invasive aspergillosis. Clin. Microbiol. Rev. **22:**447–465.
18. **Dagenais, T. R., et al.** 2008. Defects in conidiophore development and conidium-macrophage interactions in a dioxygenase mutant of *Aspergillus fumigatus*. Infect. Immun. **76:**3214–3220.
19. **Dagenais, T. R., et al.** 2010. *Aspergillus fumigatus* LaeA-mediated phagocytosis is associated with a decreased hydrophobin layer. Infect. Immun. **78:**823–829.
20. **Doyle, S.** 2009. Nonribosomal peptide synthesis: amino acids, peptides and proteins in organic chemistry, vol. 2. Wiley-VCH, Weinheim, Germany.
21. **Ejzykowicz, D. E., et al.** 2009. The *Aspergillus fumigatus* transcription factor Ace2 governs pigment production, conidiation, and virulence. Mol. Microbiol. **72:**155–169.
22. **Fox, E. M., and B. J. Howlett.** 2008. Secondary metabolism: regulation and role in fungal biology. Curr. Opin. Microbiol. **11:**481–487.
23. **Hawkins, A. R., H. K. Lamb, J. D. Moore, I. G. Charles, and C. F. Roberts.** 1993. The pre-chorismate (shikimate) and quinate pathways in filamentous fungi: theoretical and practical aspects. J. Gen. Microbiol. **139:**2891–2899.
24. **Hearn, V. M., and D. W. R. Mackenzie.** 1980. Mycelial antigens from 2 strains of *Aspergillus-Fumigatus*: an analysis by two-dimensional immunoelectrophoresis. Mykosen **23:**549–562.
25. **Hohl, T. M., et al.** 2005. *Aspergillus fumigatus* triggers inflammatory responses by stage-specific beta-glucan display. PLoS Pathog. **1:**232–240.
26. **Jin, Y., J. W. Bok, D. Guzman-de-Peña, and N. P. Keller.** 2002. Requirement of spermidine for developmental transitions in *Aspergillus nidulans*. Mol. Microbiol. **46:**801–812.
27. **Kavanagh, K., and J. P. Fallon.** 2010. *Galleria mellonella* larvae as models for studying fungal virulence. Fungal Biol. Rev. **2010:**1–5.
28. **Keller, N. P., and T. M. Hohn.** 1997. Metabolic pathway gene clusters in filamentous fungi. Fungal Genet. Biol. **21:**17–29.
29. **Kim, K. H., Y. Cho, M. La Rota, R. A. Cramer, and C. B. Lawrence.** 2007. Functional analysis of the *Alternaria brassicicola* non-ribosomal peptide synthetase gene Ab*NPS2* reveals a role in conidial cell wall construction. Mol. Plant Pathol. **8:**23–39.
30. **Krappmann, S., et al.** 2006. The *Aspergillus nidulans* F-box protein GrrA links SCF activity to meiosis. Mol. Microbiol. **61:**76–88.
31. **Kubodera, T., N. Yamashita, and A. Nishimura.** 2000. Pyrithiamine resistance gene (*ptrA*) of *Aspergillus oryzae*: cloning, characterization, and application as a dominant selectable marker for transformation. Biosci. Biotechnol. Biochem. **64:**1416–1421.
32. **Kubodera, T., N. Yamashita, and A. Nishimura.** 2002. Transformation of *Aspergillus* sp. and *Trichoderma reesei* using the pyrithiamine resistance gene (*ptrA*) of *Aspergillus oryzae*. Biosci. Biotechnol. Biochem. **66:**404–406.
33. **Laboratories, B. R.** 1986. BRL pUC host: *Escherichia coli* DH5a competent cells. Focus **8:**9.
34. **Lamb, H. K., C. R. Bagshaw, and A. R. Hawkins.** 1991. In vivo overproduction of the pentafunctional arom polypeptide in *Aspergillus nidulans* affects metabolic flux in the quinate pathway. Mol. Gen. Genet. **227:**187–196.
35. **Latge, J. P.** 1999. *Aspergillus fumigatus* and aspergillosis. Clin. Microbiol. Rev. **12:**310–312.
36. **Lee, B. N., et al.** 2005. Functional analysis of all nonribosomal peptide synthetases in *Cochliobolus heterostrophus* reveals a factor, NPS6, involved in virulence and resistance to oxidative stress. Eukaryot. Cell **4:**545–555.
37. **Levitz, S. M.** 2010. Innate recognition of fungal cell walls. PLoS Pathog. **6:**e1000758.
38. **Lipmann, F.** 1971. Attempts to map a process evolution of peptide biosynthesis. Science **173:**875–880.
39. **Maiya, S., A. Grundmann, S. M. Li, and G. Turner.** 2006. The fumitremorgin gene cluster of *Aspergillus fumigatus*: identification of a gene encoding brevianamide F synthetase. Chembiochem **7:**1062–1069.
40. **Mambula, S. S., K. Sau, P. Henneke, D. T. Golenbock, and S. M. Levitz.** 2002. Toll-like receptor (TLR) signaling in response to *Aspergillus fumigatus*. J. Biol. Chem. **277:**39320–39326.
41. **Maubon, D., et al.** 2006. AGS3, an α(1-3)glucan synthase gene family member of *Aspergillus fumigatus*, modulates mycelium growth in the lung of experimentally infected mice. Fungal Genet. Biol. **43:**366–375.
42. **Medzhitov, R., and C. A. Janeway.** 2000. How does the immune system distinguish self from nonself? Semin. Immunol. **12:**185–188.
43. **Meier, A., et al.** 2003. Toll-like receptor (TLR) 2 and TLR4 are essential for *Aspergillus*-induced activation of murine macrophages. Cell. Microbiol. **5:**561–570.
44. **Moon, Y. S., et al.** 2008. *Agrobacterium*-mediated disruption of a nonribosomal peptide synthetase gene in the invertebrate pathogen *Metarhizium anisopliae* reveals a peptide spore factor. Appl. Environ. Microbiol. **74:**4366–4380.
45. **Mootz, H. D., D. Schwarzer, and M. A. Marahiel.** 2002. Ways of assembling complex natural products on modular nonribosomal peptide synthetases. Chembiochem **3:**491–504.
46. **Nett, J. E., H. Sanchez, M. T. Cain, and D. R. Andes.** 2010. Genetic basis of *Candida* biofilm resistance due to drug-sequestering matrix glucan. J. Infect. Dis. **202:**171–175.
47. **Nielsen, K. F., J. M. Mogensen, M. Johansen, T. O. Larsen, and J. C. Frisvad.** 2009. Review of secondary metabolites and mycotoxins from the *Aspergillus niger* group. Anal. Bioanal. Chem. **395:**1225–1242.
48. **Nielsen, K. F., and J. Smedsgaard.** 2003. Fungal metabolite screening: database of 474 mycotoxins and fungal metabolites for dereplication by standardized liquid chromatography-UV-mass spectrometry methodology. J. Chromatogr. A **1002:**111–136.
49. **Nielsen, M. L., L. Albertsen, G. Lettier, J. B. Nielsen, and U. H. Mortensen.** 2006. Efficient PCR-based gene targeting with a recyclable marker for *Aspergillus nidulans*. Fungal Genet. Biol. **43:**54–64.
50. **Nierman, W. C., et al.** 2005. Genomic sequence of the pathogenic and allergenic filamentous fungus *Aspergillus fumigatus*. Nature **438:**1151–1156.
51. **Oide, S., et al.** 2006. NPS6, encoding a nonribosomal peptide synthetase involved in siderophore-mediated iron metabolism, is a conserved virulence determinant of plant pathogenic ascomycetes. Plant Cell **18:**2836–2853.
52. **Perrin, R. M., et al.** 2007. Transcriptional regulation of chemical diversity in *Aspergillus fumigatus* by LaeA. PLoS Pathog. **3:**508–517.
53. **Pfaffl, M. W.** 2001. A new mathematical model for relative quantification in real-time RT-PCR. Nucleic Acids Res. **29:**e45.
54. **Pfaller, M., et al.** 2011. Comparison of the broth microdilution methods of the European Committee on Antimicrobial Susceptibility Testing and the Clinical and Laboratory Standards Institute for testing itraconazole, posaconazole, and voriconazole against *Aspergillus* isolates. J. Clin. Microbiol. **49:**1110–1112.
55. **Ram, A. F. J., and F. M. Klis.** 2006. Identification of fungal cell wall mutants using susceptibility assays based on Calcofluor white and Congo red. Nat. Protoc. **1:**2253–2256.
56. **Reeves, E. P., C. G. M. Messina, S. Doyle, and K. Kavanagh.** 2004. Correlation between gliotoxin production and virulence of *Aspergillus fumigatus* in *Galleria mellonella*. Mycopathologia **158:**73–79.
57. **Reeves, E. P., et al.** 2006. A nonribosomal peptide synthetase (Pes1) confers protection against oxidative stress in *Aspergillus fumigatus*. FEBS J. **273:**3038–3053.
58. **Reiber, K., et al.** 2005. The expression of selected non-ribosomal peptide synthetases in *Aspergillus fumigatus* is controlled by the availability of free iron. FEMS Microbiol. Lett. **248:**83–91.
59. **Romano, J., et al.** 2006. Disruption of the *Aspergillus fumigatus* ECM33 homologue results in rapid conidial germination, antifungal resistance, and hypervirulence. Microbiology **152:**1919–1928.
60. **Schrettl, M., et al.** 2007. Distinct roles for intra- and extracellular siderophores during *Aspergillus fumigatus* infection. PLoS Pathog. **3:**1195–1207.
61. **Schrettl, M., et al.** 2010. Self-protection against gliotoxin: a component of the gliotoxin biosynthetic cluster, GliT, completely protects *Aspergillus fumigatus* against exogenous gliotoxin. PLoS Pathog. **6:**e1000952.
62. **Siednienko, J., A. Halle, K. Nagpal, D. T. Golenbock, and S. M. Miggin.** 2010. TLR3-mediated IFN-β gene induction is negatively regulated by the TLR adaptor MyD88 adaptor-like. Eur. J. Immunol. **40:**3150–3160.
63. **Slater, J. L., L. Gregson, D. W. Denning, and P. A. Warn.** 2010. Pathogenicity

of *Aspergillus fumigatus* mutants assessed in *Galleria mellonella* matches that in mice. Med. Mycol. doi:10.3109/13693786.2010.523852.
64. **Smedsgaard, J.** 1997. Micro-scale extraction procedure for standardized screening of fungal metabolite production in cultures. J. Chromatogr. A **760:**264–270.
65. **Stack, D., A. Frizzell, K. Tomkins, and S. Doyle.** 2009. Solid-phase 4′-phosphopantetheinylation: fungal thiolation domains are targets for chemoenzymatic modification. Bioconj. Chem. **20:**1514–1522.
66. **Stack, D., C. Neville, and S. Doyle.** 2007. Nonribosomal peptide synthesis in *Aspergillus fumigatus* and other fungi. Microbiology **153:**1297–1306.
67. **Steele, C., et al.** 2005. The beta-glucan receptor dectin-1 recognizes specific morphologies of *Aspergillus fumigatus*. PLoS Pathog. **1:**323–334.
68. **Sugui, J. A., et al.** 2007. Gliotoxin is a virulence factor of *Aspergillus fumigatus*: *gliP* deletion attenuates virulence in mice Immunosuppressed with hydrocortisone. Eukaryot. Cell **6:**1562–1569.
69. **Thau, N., et al.** 1994. Rodletless mutants of *Aspergillus-Fumigatus*. Infect. Immun. **62:**4380–4388.
70. **Tilburn, J., et al.** 1983. Transformation in *Aspergillus nidulans*. Heredity **51:**519–520.
71. **Tsitsigiannis, D. I., et al.** 2005. Aspergillus cyclooxygenase-like enzymes are associated with prostaglandin production and virulence. Infect. Immun. **73:**4548–4559.
72. **Tsoni, S. V., and G. D. Brown.** 2008. β-Glucans and dectin-1, p. 45–60. *In* Year in immunology 2008, vol. 1143. Blackwell Publishing, Oxford, England.
73. **Valdés-Santiago, L., J. A. Cervantes-Chávez, and J. Ruiz-Herrera.** 2009. *Ustilago maydis* spermidine synthase is encoded by a chimeric gene, required for morphogenesis, and indispensable for survival in the host. FEMS Yeast Res. **9:**923–935.
74. **Wang, J. E., et al.** 2001. Involvement of CD14 and Toll-like receptors in activation of human monocytes by *Aspergillus fumigatus* hyphae. Infect. Immun. **69:**2402–2406.
75. **Werner, J. L., et al.** 2009. Requisite role for the dectin-1 β-glucan receptor in pulmonary defense against *Aspergillus fumigatus*. J. Immunol. **182:**4938–4946.
76. **Zhao, J., and X. Y. Wu.** 2008. *Aspergillus fumigatus* antigens activate immortalized human corneal epithelial cells via Toll-like receptors 2 and 4. Curr. Eye Res. **33:**447–454.

Editor: G. S. Deepe, Jr.